

Synthesis and characterization of magnetic bromochromate hybrid nanomaterials with triphenylphosphine surface-modified iron oxide nanoparticles and their catalytic application in multicomponent reactions

Cite this: *RSC Adv.*, 2014, 4, 29765

Ali Maleki,* Rahmatollah Rahimi, Saied Maleki and Negar Hamidi

In this work, the preparation of a new magnetic hybrid core-shell nanomaterial is reported in four steps. The magnetic Fe_3O_4 nanoparticles were synthesized *via* a simple hydrothermal system. Tetraethyl orthosilicate was used as a source of SiO_2 for the creation of $\text{Fe}_3\text{O}_4@\text{SiO}_2$ core-shell nanoparticles. The subsequent functionalization of $\text{Fe}_3\text{O}_4@\text{SiO}_2$ was achieved by using (3-chloropropyl)trimethoxysilane and triphenylphosphine. Finally, immobilization of the anionic part including the $[\text{CrO}_3\text{Br}]^-$ was carried out to obtain $\text{Fe}_3\text{O}_4@\text{SiO}_2@\text{PPh}_3@[\text{CrO}_3\text{Br}]$. The structure and morphology of the prepared nanocatalyst was characterized by using elemental analysis, scanning electron microscopy (SEM), transmission electron microscopy (TEM), X-ray fluorescence (XRF), X-ray diffraction (XRD), Fourier transform infrared (FT-IR) and a vibrating sample magnetometer (VSM). The prepared catalyst showed efficient activity as an heterogeneous catalyst in the synthesis of 1,4-dihydropyridine derivatives at room temperature. Moreover, the catalyst can be readily recovered by simple magnetic decantation and can be recycled several times with no significant loss of catalytic activity.

Received 17th May 2014
Accepted 11th June 2014

DOI: 10.1039/c4ra04654d

www.rsc.org/advances

Introduction

Heterogeneous catalysts are especially interesting in academic and industrial research, mainly because of their simple separation from a mixture of products and due to their reusability.¹ However, the heterogeneous catalysts broadly need tedious preparation and/or separation processes, and there is a necessity to obtain new materials with special properties such as magnetism in order to overcome these weaknesses. Magnetic nanoparticles are an important class of nanostructures materials of current interest, mostly due to their advanced technological and medical applications. Among the various magnetic nanoparticles, Fe_3O_4 nanoparticles are arguably the most extensively studied and have recently emerged as promising supports for the immobilization of core-shell metal nanoparticles. Fe_3O_4 -supported nanocatalysts can be separated from the reaction medium by an external permanent magnet.^{2–5} In general, in order to inhibit direct contact between magnetite nanoparticles and also to prepare a suitable surface for the modification of magnetite nanoparticles, a coating of the surface with silica shell is necessary. A silica surface can be easily functionalized with various organic groups for favourable

purposes such as applications as an adsorbent, catalysis support, and enzyme immobilization.⁶

Multicomponent reactions (MCRs) are one of the most effective and important tools in modern synthetic organic chemistry. These reactions can make products by forming multiple new bonds *via* a one-pot process without separating the intermediates. Efficiency, atom economy and simplicity are the key features that make them a common area of research in modern organic reactions.⁷

1,4-Dihydropyridine (DHP) derivatives contain a large family of medicinally important compounds with diverse pharmacological and therapeutic properties, such as a vasodilator, hepatoprotective, antiatherosclerotic, bronchodilator, antitumor, geroprotective and in antidiabetic activities.⁸ Although the synthesis of DHPs has been endorsed by a variety of homogeneous and heterogeneous acid catalysts, some of these methods suffer from limited scope, such as low yields, long reaction times, expensive catalysts and difficult work-up procedures.^{9,10}

In the present work, we aimed to prepare a magnetically recoverable nanocatalyst, in which bromochromate was immobilized on triphenylphosphine-functionalized silica-coated iron oxide nanoparticles. One of the advantages of this system is the relatively strong chemical interaction between the bromochromate anion and the phosphonium groups functionalized on the surface of the magnetite nanoparticles. Moreover, due to the presence of the magnetite core, the

Department of Chemistry, Iran University of Science and Technology, Tehran 16846-13114, Iran. E-mail: maleki@iust.ac.ir; Fax: +98-21-73021584; Tel: +98-21-77240640-50

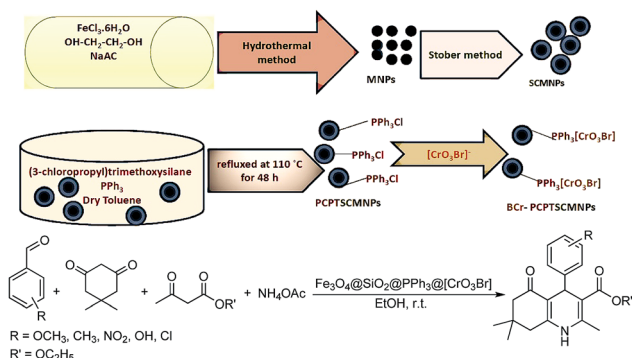


Fig. 1 Preparation and catalytic application of $\text{Fe}_3\text{O}_4\text{@SiO}_2\text{@PPh}_3\text{@[CrO}_3\text{Br}]$.

prepared hybrid nanomaterials have superparamagnetic properties, which make them easily separable in potential applications in various fields, such as for oxidation of olefins and alcohols and for multicomponent reactions as magnetically recoverable catalysts. The catalytic activity of $\text{Fe}_3\text{O}_4\text{@SiO}_2\text{@PPh}_3\text{@[CrO}_3\text{Br}]$ was investigated in a Hantzsch-DHPs synthesis *via* a four-component reaction strategy. Herein, DHP derivatives are prepared by a MCR of dimedone, a β -ketoester, an aldehyde, and ammonium acetate (Fig. 1). In comparison with other catalysts, this nanocatalyst has both metal ions and triphenylphosphine; therefore, it has phase transfer catalyst properties. The phase transfer catalyst property of the catalyst supports both a reduced time and increased yield of reaction. Therefore, briefly, these properties of the new catalyst offer several advantages, such as high yields, short reaction time, simple work-up procedure and reusability of the catalyst.

Experimental

Materials and instrumentation

All chemicals were purchased from Merck, Fluka and Aldrich. Melting points were measured on an Electrothermal 9200 apparatus and are uncorrected. Fourier transform infrared (FT-IR) spectra were registered using a Perkin-Elmer Spectrum RXI FT-IR spectrometer using pellets of the nanomaterials diluted with KBr. Chemical analyses were performed with Philips-PW1480 X-ray fluorescence (XRF) spectrometer. The crystalline phase of the nanoparticles were recognized by X-ray diffraction (XRD) measurements using Cu K_α radiation ($\lambda = 1.54 \text{ \AA}$) on a Philips-PW1800 diffractometer in the 2θ range of $4-90^\circ$. Scanning electron microscopy (SEM) images of the samples were taken with a Zeiss-DSM 960A microscope with an attached camera. Transmission electron microscopy (TEM) images were obtained through a Zeiss EM 900 electron microscope operating at 80 kV. Magnetic susceptibility measurements were carried out using a vibrating sample magnetometer (BHV-55, Riken, Japan) in the magnetic field range of $-10\,000$ Oe to $+10\,000$ Oe at room temperature. The Cr leaching content of the catalyst was measured by inductively coupled plasma (ICP) by Shimadzu S 7000.

Preparations of Fe_3O_4 nanoparticles (MNPs)

Fe_3O_4 magnetite nanoparticles were provided by a known procedure.^{11,12} In general, $\text{FeCl}_3 \cdot 6\text{H}_2\text{O}$ (2.7 g) was dissolved in ethylene glycol (70 mL) to form a clear solution, followed by the addition of NaOAc (7.2 g). Then, the mixture was stirred vigorously for 30 min and sealed in a 100 mL Teflon-lined stainless-steel autoclave. Next, the autoclave was heated and maintained at 200°C for 8 h, and then cooled to room temperature. The black Fe_3O_4 particles were washed several times with ethanol and dried at 60°C in a vacuum oven.

Preparation of silica-coated magnetite nanoparticles ($\text{Fe}_3\text{O}_4\text{@SiO}_2$) (SCMNPs)

The interlayers of SiO_2 were prepared through a modified Stober method.^{13–20} In a typical process, as-prepared Fe_3O_4 particles (1.5 g) were dispersed in a mixture of ethanol (120 mL), deionized water (30 mL) and concentrated ammonia aqueous solution (25 wt%, 3.8 mL) by ultrasonication for 15 min. Next, 5 mL of tetraethyl orthosilicate (TEOS) was added dropwise. After stirring for 12 h, the products were collected and washed with deionized water and then dried under vacuum at 60°C for further use.

Functionalizing of silica-coated magnetite nanoparticles $\text{Fe}_3\text{O}_4\text{@SiO}_2$ (SCMNPs) with triphenylphosphine (PCPTSCMNPs)

Initially, 1 g of silica-coated magnetite nanoparticles were dispersed in dry toluene (80 mL) by ultrasonication.²⁰ Then, (3-chloropropyl)trimethoxysilane (5 g) and triphenylphosphine (8 g) were added in dispersed nanoparticles, and the mixture was refluxed at 110°C for 48 h. After that, the solid product was cooled and isolated by a magnet, washed twice with deionized water (100 mL) and ethanol (100 mL), and dried in vacuum at 60°C .

Synthesis of bromochromate (VI), $[\text{CrO}_3\text{Br}]$

To a solution of CrO_3 (0.01 mol/100 mL) in H_2O , a solution of (0.01 mol) in HBr was added with stirring at room temperature until an orange solution was formed.

Synthesis of $\text{Fe}_3\text{O}_4\text{@SiO}_2\text{@PPh}_3\text{@[CrO}_3\text{Br}]$ (BCr-PCPTSCMNPs)

$\text{Fe}_3\text{O}_4\text{@SiO}_2\text{@PPh}_3$ (1 g) was dispersed into 100 mL of distilled water and $[\text{CrO}_3\text{Br}]^-$ (0.1 mmol) was added. The resultant mixture was stirred at room temperature for 24 h. After that, the resulting $\text{Fe}_3\text{O}_4\text{@SiO}_2\text{@PPh}_3\text{@[CrO}_3\text{Br}]$ was washed with water and diethyl ether thoroughly and dried in a vacuum oven at 60°C .

General procedure for the preparation of 1,4-dihydropyridines

To a mixture of dimedone (1 mmol), ethylacetoacetate (1 mmol) and BCr-PCPTSCMNPs (0.01 g) in EtOH (5 mL), aldehyde (1 mmol) and ammonium acetate (1 mmol) were added at room temperature. The reaction mixture was stirred at room

temperature until the reaction was completed (monitored by TLC). Then, the mixture was cooled to room temperature and BCr-PCPTSCMNPs were separated by an external magnet. After evaporation of the solvent, the solid product was filtered and recrystallized from EtOH to obtain the pure products. The pure products weight and yields were obtained *via* calculation.

Results and discussion

Preparation of magnetite bromochromate nanomaterials

The order of steps in the immobilization of the magnetite core-shell nanoparticles is shown in Fig. 1. First, Fe_3O_4 magnetic nanoparticles were synthesized by a hydrothermal procedure. Next, the external surface of the MNPs was coated with silica shell to create SCMNPs. Sturdy materials such as silica as coupling layers are used in the preparation of magnetically recyclable nanocatalysts (MRNCs) frequently. The hard coupling layers can act as anchoring sites for the nanocatalysts or the precursors of the nanocatalysts to support them, and thus combine both superparamagnetic components and nanocatalysts. Magnetic cores are completely protected by the solid silica outer layer against the external environment; thus, MRNCs can be applied in relatively difficult reaction conditions (strong acidic and strong oxidizing).

Moreover, the silica surface can be functionalized using a multiplicity of known surface modifiers. Compared with the hard coupling layer materials indicated above, soft organic molecules with several functional groups, such as $-\text{SH}$, $-\text{COOH}$, $-\text{OH}$, $-\text{NH}_2$ and pyrrole rings, can be more simply attached to the surface of magnetic components, as well as to catalytic active species, through covalent bonds, coordination bonds, and electrostatic interaction. Most of the time, hard and soft coupling layers were used together for the convenient fabrication of MRNCs. The hard coupling layers mainly serve as a protective shell for the magnetic components, while the soft coupling layers with multiple functional groups act as anchoring sites for the catalytic active species. The most frequently used combination of hard and soft buffer layers is silica and silane coupling agents or polymers. The action of the silanol groups of SCMNPs with triphenylphosphonium (3-chloropropyl)trimethoxysilane produced PCPTSCMNPs.

The next step involved the reaction of the PCPTSCMNPs groups with bromochromate to yield the magnetite bromochromate nanomaterials BCr-PCPTSCMNPs. In this step, phosphonium groups give positively charged cations, which bonds electrostatically to the bromochromate. As a result, the excess of bromochromate was removed by washing the resulting materials with water. The attached bromochromate anions are established on the surface of modified magnetite and could not be leached to aqueous solution.^{6,21}

Characterization of the prepared magnetite-bromochromate nanomaterials

In order to exhibit the surface modification of the magnetite nanoparticles and preparation of the magnetite bromochromate nanomaterials, the FT-IR spectra of the prepared MNPs,

SCMNPs, PCPTSCMNPs, BCr-PCPTSCMNPs are shown in Fig. 2. As shown in Fig. 2a, Fe_3O_4 usually presents bands at ~ 430 and 576 cm^{-1} due to Fe–O vibrations in octahedral and tetrahedral sites, respectively.^{22,23} The strong absorption band at 1095 cm^{-1} was ascribed to Si–O–Si vibrations, demonstrating the presence of SiO_2 .^{24,25} The weak bond at 810 cm^{-1} is characteristic of Si–O–Fe. These outcomes indicate that SiO_2 is immobilized on the surfaces of $\text{Fe}_3\text{O}_4@ \text{SiO}_2$ core-shells (Fig. 2b).^{16–19} The presence of propyl and triphenylphosphine were verified by the stretching vibrations appearing at about 2830 , 2900 cm^{-1} in the FT-IR spectrum of PCPTSCMNPs (Fig. 2c).^{6,26} In Fig. 2d, the presence of the absorption bands at 770 , 805 , 895 , 905 ($\nu_{\text{asymmetric}} \text{Cr}=\text{O}$ (A₁)), 940 ($\nu_{\text{symmetric}} \text{Cr}=\text{O}$ (E)) demonstrate the immobilization of the bromochromate.

Chemical analysis of the $\text{Fe}_3\text{O}_4@ \text{SiO}_2@ \text{PPh}_3@ [\text{CrO}_3\text{Br}]$ by X-ray fluorescence (XRF) is shown in Table 1. As can be seen in this table, the quantity of chromium is nearly 0.39%, which confirms the immobilization amount of $[\text{CrO}_3\text{Br}]^-$ was 0.0075 mol/100 g. Loss on ignition (L.O.I.) calculations indicate the quantity of organic matter in $\text{Fe}_3\text{O}_4@ \text{SiO}_2@ \text{PPh}_3@ [\text{CrO}_3\text{Br}]$.

The crystalline structure of the magnetite bromochromate nanoparticles is specified by XRD as demonstrated in Fig. 3. The results are in accord with standard patterns of an inverse cubic spinel magnetite (Fe_3O_4) crystal structure, showing six diffraction peaks at 2θ about 29.70° (2 2 0), 35.21° (3 1 1), 42.96° (4 0 0), 53.53° (4 2 2), 56.97° (5 1 1) and 62.52° (4 4 0) (JCPDS Card no. 19-0629).^{27,28} The strong and sharp peaks indicated that Fe_3O_4 crystals are highly crystalline. As can be seen, the resultant nanomaterials show only the typical diffraction peaks of magnetite nanoparticles, and there are no specific peaks for bromochromate. This illustrates that the bromochromate species are well dispersed on the surface of PCPTSCMNPs, and there is no longer any crystalline phase of bromochromate in the resultant nanomaterials. The average crystallite size of nanoparticles was also determined from X-ray line broadening using the Debye–Scherrer formula ($D = 0.9\lambda/\beta \cos \theta$, where D is

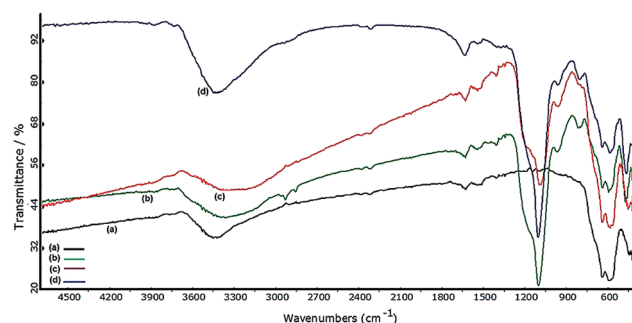


Fig. 2 FT-IR spectra of: (a) Fe_3O_4 , (b) $\text{Fe}_3\text{O}_4@ \text{SiO}_2$, (c) $\text{Fe}_3\text{O}_4@ \text{SiO}_2@ \text{PPh}_3$ and (d) $\text{Fe}_3\text{O}_4@ \text{SiO}_2@ \text{PPh}_3@ [\text{CrO}_3\text{Br}]$.

Table 1 XRF results of $\text{Fe}_3\text{O}_4@ \text{SiO}_2@ \text{PPh}_3@ [\text{CrO}_3\text{Br}]$

Element	Fe	Si	O	Cr	P	L.O.I.
Percentage	23.28	26.85	32.80	0.39	1.92	14.76

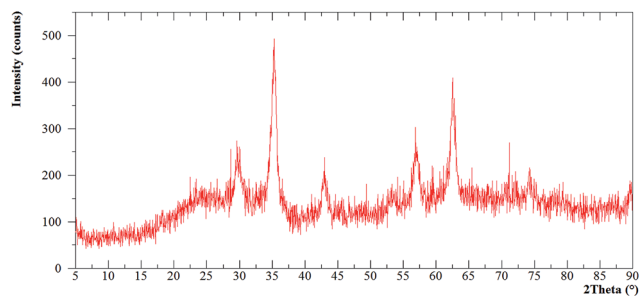


Fig. 3 XRD pattern of $\text{Fe}_3\text{O}_4@\text{SiO}_2@\text{PPh}_3@[\text{CrO}_3\text{Br}]$.

the average crystalline size, λ is the X-ray wavelength used, β is the angular line width at half maximum intensity and θ is the Bragg's angle). For the 3 1 1 reflection, the average size of the Fe_3O_4 NPs was calculated to be around 24 nm.^{7,29}

The morphology and size details of the nanocatalyst were investigated by SEM measurement, which is illustrated in Fig. 4a. The SEM image of pure Fe_3O_4 indicated that the mean diameter of the Fe_3O_4 particles is around 15 nm. Aggregation enhances the size of the observed nanoparticles as observed in the SEM image. Fig. 4b and c show that the iron oxide nanoparticles have a core-shell mode and spherical morphology. Fig. 4d–f show images of the obtained $\text{Fe}_3\text{O}_4@\text{SiO}_2@\text{PPh}_3@[\text{CrO}_3\text{Br}]$.

The TEM images shown in Fig. 5 indicated that the silica-magnetite composites made as supports for the catalyst had good spherical morphologies and regular core-shell structures.

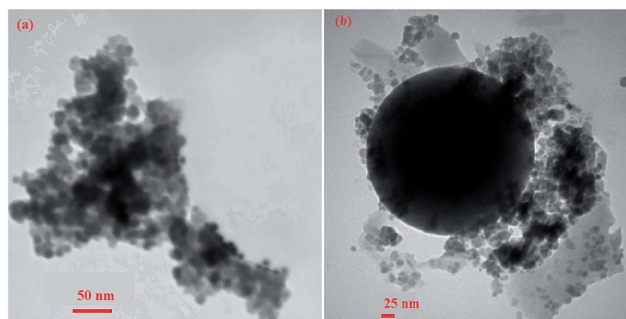


Fig. 5 TEM images of $\text{Fe}_3\text{O}_4@\text{SiO}_2$.

The average particle size of $\text{Fe}_3\text{O}_4@\text{SiO}_2$ was about 15 nm. During the seeded sol-gel method, the thickness of the silica shells of the $\text{Fe}_3\text{O}_4@\text{SiO}_2$ particles can be appropriately adapted by controlling the addition amount of silica source (TEOS). With the growing of the particle sizes, the magnetic properties of the particles reduces, which was inadequate for the separation of the catalyst from the reaction mixture. Usually, compared with the large-size support solid, nanoparticles with small particle sizes have a larger specific surface area and better dispersion in the solvent, which can have useful effects for the catalysis.³⁰

Magnetic measurements were carried out using a vibrating sample magnetometer (VSM) at 300 K. The magnetization curves measured for the Fe_3O_4 nanoparticles and for $\text{Fe}_3\text{O}_4@\text{SiO}_2@\text{PPh}_3@[\text{CrO}_3\text{Br}]$ are compared in Fig. 6. There was no hysteresis in the magnetization for the two examined nanoparticles. As can be seen in Fig. 6, the values of the saturation magnetization were 53 emu g^{-1} for Fe_3O_4 nanoparticles, 37 emu g^{-1} for $\text{Fe}_3\text{O}_4@\text{SiO}_2$, 31 emu g^{-1} for $\text{Fe}_3\text{O}_4@\text{SiO}_2@\text{PPh}_3$ and 28 emu g^{-1} for $\text{Fe}_3\text{O}_4@\text{SiO}_2@\text{PPh}_3@[\text{CrO}_3\text{Br}]$. The reduction of nearly 25 emu g^{-1} in the saturation magnetization suggests the presence of some $\text{SiO}_2@\text{PPh}_3@[\text{CrO}_3\text{Br}]$ on the surface of the magnetic supports. Even with this reduction in the saturation magnetization, the catalyst still can be competently and easily separated from the solution with the use of an external magnetic force.

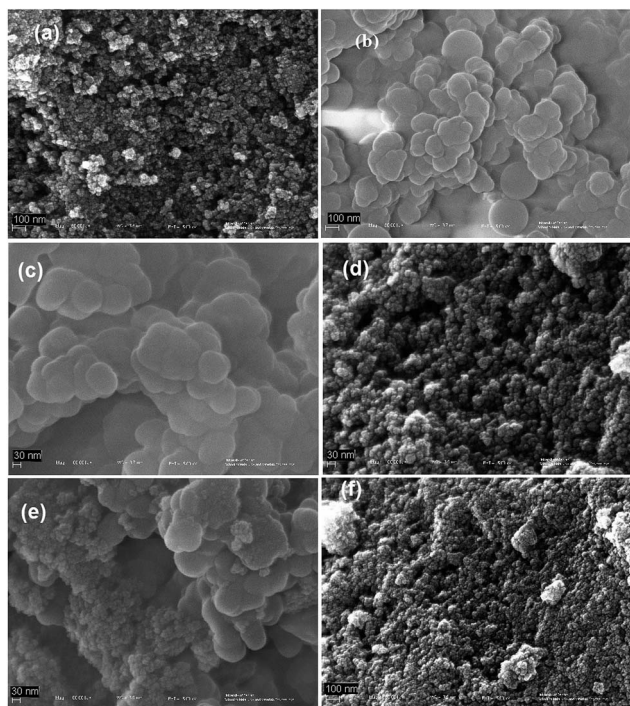


Fig. 4 SEM images of: (a) Fe_3O_4 , (b and c) $\text{Fe}_3\text{O}_4@\text{SiO}_2$, (d–f) $\text{Fe}_3\text{O}_4@\text{SiO}_2@\text{PPh}_3@[\text{CrO}_3\text{Br}]$.

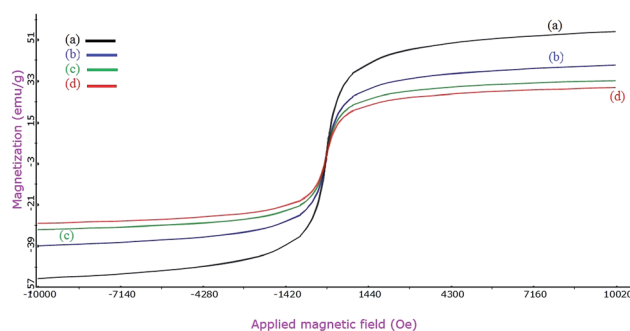


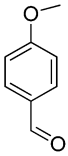
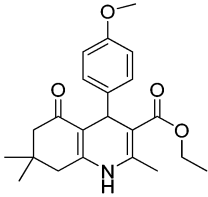
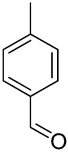
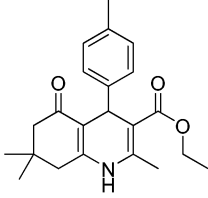
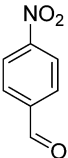
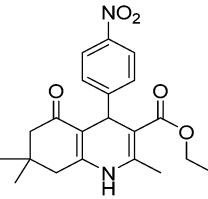
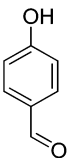
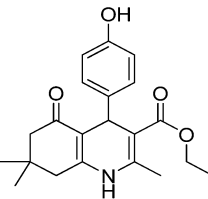
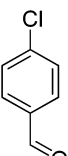
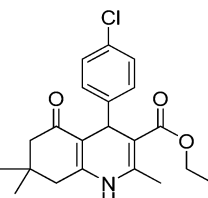
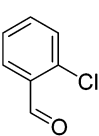
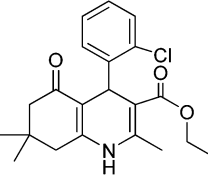
Fig. 6 Magnetization curves of (a) Fe_3O_4 , (b) $\text{Fe}_3\text{O}_4@\text{SiO}_2$, (c) $\text{Fe}_3\text{O}_4@\text{SiO}_2@\text{PPh}_3$ (d) $\text{Fe}_3\text{O}_4@\text{SiO}_2@\text{PPh}_3@[\text{CrO}_3\text{Br}]$.

Preparation of 1,4-DHPs in the presence of $\text{Fe}_3\text{O}_4@\text{SiO}_2@\text{PPh}_3@[\text{CrO}_3\text{Br}]$

To investigate the catalytic activity of the prepared nanocatalyst, a one-pot four-component synthesis of 1,4-DHP derivatives through the Hantzsch reaction of dimedone, β -ketoesters, aldehydes, and ammonium acetate was carried out in EtOH at room temperature (Table 2). This protocol had the ability to endure a variety of functional groups such as hydroxyl, methoxy,

methyl, nitro and halides under the reaction conditions. Both the electron-rich and electron-deficient aldehydes worked well and led to the target products in high yields. The structures of all the products were recognized from their melting points and FT-IR spectral data. After the fifth cycle, the Cr leaching of the catalyst was also determined. ICP analysis of the clear filtrate showed that the Cr content was less than 0.11 ppm, which

Table 2 Synthesis of 1,4-dihydropyridines in the presence of $\text{Fe}_3\text{O}_4@\text{SiO}_2@\text{PPh}_3@[\text{CrO}_3\text{Br}]$ nanocatalyst^a

Entry	Aldehyde	Product	Time (min)	Run, yield ^b (%)	IR, KBr (cm^{-1})	Mp ($^{\circ}\text{C}$)	Lit. mp ($^{\circ}\text{C}$)
1			45	1, 91 2, 90 3, 89 4, 88 5, 85	3275, 3200, 2957, 1705, 1647, 1605, 1497, 1382, 1217, 1032, 849, 536 (ref. 31) ^c	255	258–260 (ref. 33)
2			50	1, 96 2, 94 3, 94 4, 93 5, 90	3276, 3207, 3078, 2960, 1701, 1647, 1604, 1492, 1380, 1280, 1217, 1072, 848, 554 (ref. 31)	258–260	258–260 (ref. 34)
3			60	1, 93 2, 92 3, 91 4, 89 5, 88	3278, 3199, 3076, 2960, 1701, 1643, 1608, 1517, 1488, 1344, 1218, 1072, 836, 696 (ref. 32)	240	240–242 (ref. 35)
4			48	1, 94 2, 93 3, 91 4, 90 5, 89	3390, 3082, 2958, 1700, 1645, 1600, 1483, 1379, 1220, 1074, 782, 684, 540 (ref. 31)	235–236	232–234 (ref. 35)
5			60	1, 89 2, 87 3, 86 4, 85 5, 84	3274, 3203, 3076, 2960, 1704, 1647, 1604, 1490, 1382, 1278, 1215, 1070, 840, 530 (ref. 32)	240–242	241–243 (ref. 36)
6			60	1, 87 2, 86 3, 84 4, 82 5, 81	3292, 3209, 2960, 1720, 1637, 1608, 1483, 1380, 1215, 1072, 754, 588 (ref. 31)	202–203	202–205 (ref. 37)

^a Reaction conditions: aldehyde (1 mmol), dimedone (1 mmol), ethyl acetoacetate (1 mmol), ammonium acetate (1 mmol), catalyst (0.01 g), EtOH (5 mL), r.t. ^b Isolated yield. ^c IR active modes: 3275 (N–H, s), 3200 (C–H, Ar, s), 2975 (C–H, CH_3 , s), 1705 (C=O, ester, s), 1647 (C=O, ketone, s), 1605 and 1497 (C=C, Ar, s), 1217 and 1032 (C–O, s), 849 cm^{-1} (C–H, b) [s: strong; b: broad].

Table 3 Synthesis of 1,4-dihydropyridines in the presence of various catalysts^a

Entry	Catalyst	Solvent	Temp. (°C)	Time (min)	Yield ^b (%)	Lit.
1	Cellulose sulfuric acid	H ₂ O	100	120–300	78–92	10
2	PPh ₃	C ₂ H ₅ OH	Reflux	300	72	38
3	MgAl ₂ @hydrotalcites	CH ₃ CN	r.t.	390	32–75	39
4	NaHSO ₄ @SiO ₂	CH ₃ CN	r.t.	300–480	75–90	40
5	Fe ₃ O ₄ @SiO ₂	C ₂ H ₅ OH	r.t.	240	60	Present work
6	Fe ₃ O ₄ @SiO ₂ @PPh ₃	C ₂ H ₅ OH	r.t.	180	70	Present work
7	Fe ₃ O ₄ @SiO ₂ @PPh ₃ @[CrO ₃ Br]	C ₂ H ₅ OH	r.t.	50	96	Present work

^a Reaction conditions: 4-methylbenzaldehyde (1 mmol), dimedone (1 mmol), ethyl acetoacetate (1 mmol), ammonium acetate (1 mmol), catalyst (0.01 g), and solvent (5 mL). ^b Isolated yield.

shows that the BCr-PCPTSCM NPs catalyst was very stable and could tolerate this reaction.

As indicated in Table 3, to compare the efficiency of this new nanocatalyst, we carried out a model reaction in the presence of various catalysts. Fe₃O₄@SiO₂ and Fe₃O₄@SiO₂@PPh₃ needed longer reaction times than Fe₃O₄@SiO₂@PPh₃@[CrO₃Br] at room temperature. Previously, PPh₃ was reported as a catalyst for this reaction, in which the reaction time was between 120 and 300 min and reflux conditions were required.³⁸ In addition, the present catalyst is capable of catalyzing the four-component reaction but the other ones were applied in three-component reactions.

Reusability of the catalyst

The reusability of the catalyst is very important in large scale industrial synthetic processes. The recyclability of the catalyst was screened in the synthesis of 1,4-DHPs. Separating the catalyst from the reaction mixture was simple. When the reaction was complete, the catalyst was recovered nearly quantitatively from the reaction flask by an external magnet and was subsequently reused in several runs. As illustrated in Table 2, it demonstrated nearly no loss of activity after five successive runs. The activities of the catalysts reduced though due to leaching of the active composition [CrO₃Br][−]. The reaction for regenerating the catalysts was carried out in water with [CrO₃Br][−].

Conclusions

This work has explained the preparation of functionalized magnetic nanomaterials by reacting triphenylphosphine-modified silica-coated magnetite nanoparticles with bromochromate anion. The XRD pattern, XRF results and FT-IR spectra of the magnetite catalysts show that the [CrO₃Br][−] was immobilized onto the surface of the Fe₃O₄ magnetite nanoparticles. This catalytic system can efficiently catalyse the preparation of 1,4-dihydropyridines at room temperature. Moreover, the catalyst can be easily separated from the reaction system by an external magnet, and reused several times.

Acknowledgements

The authors gratefully acknowledge the financial support from the Iran National Science Foundation (INSF), partial support

from the Iran University of Science and Technology, and the reviewers for valuable comments and suggestions.

Notes and references

- For a review, see: M. J. Climent, A. Corma and S. Iborra, *RSC Adv.*, 2012, **2**, 16–58.
- S. Prasad and B. Satyanarayana, *J. Mol. Catal. A: Chem.*, 2013, **370**, 205–209.
- J. K. Lim and S. A. Majetich, *Nano Today*, 2013, **8**, 98–113.
- N. C. Bigall, W. J. Parak and D. Dorfs, *Nano Today*, 2012, **7**, 282–296.
- A. Maleki and M. Kamalzare, *Catal. Commun.*, 2014, **53**, 67.
- M. M. Farahani, J. Movassagh, F. Taghavi, P. Eghbali and F. Salimi, *Chem. Eng. J.*, 2012, **184**, 342–346.
- M. V. Marques, M. M. Ruthner, L. A. M. Fontoura and D. Russowsky, *J. Braz. Chem. Soc.*, 2012, **23**, 171–179.
- M. N. Esfahani, S. J. Hoseini, M. Montazerzohori, R. Mehrabi and H. Nasrabadi, *J. Mol. Catal. A: Chem.*, 2014, **382**, 99–105.
- F. Tamadon and S. Moradi, *J. Mol. Catal. A: Chem.*, 2013, **370**, 117–122.
- J. Safari, S. H. Banitaba and S. D. Khalili, *J. Mol. Catal. A: Chem.*, 2011, **335**, 46–50.
- M. Zhang, J. Zheng, Y. Zheng, J. Xu, X. He, L. Chen and Q. Fang, *RSC Adv.*, 2013, **3**, 13818–13824.
- M. Xie, F. Zhang, Y. Long and J. Ma, *RSC Adv.*, 2013, **3**, 10329–10334.
- R. B. N. Baig and R. S. Varma, *RSC Adv.*, 2014, **4**, 6568–6572.
- J. Safari and Z. Zarnegar, *J. Mol. Catal. A: Chem.*, 2013, **379**, 269–276.
- J. Davarpanah and A. R. Kiasat, *Catal. Commun.*, 2013, **42**, 98–103.
- A. Maleki, *Tetrahedron*, 2012, **68**, 7827–7833.
- A. Maleki, *Tetrahedron Lett.*, 2013, **54**, 2055–2059.
- A. Maleki, *Helv. Chim. Acta*, 2014, **97**, 587–593.
- Z. Dong, X. Tian, Y. Chen, Y. Guo and J. Ma, *RSC Adv.*, 2013, **3**, 1082–1088.
- Y. Jiang, C. Guo, H. Xia, I. Mahmood, C. Liu and H. Liu, *J. Mol. Catal. B: Enzym.*, 2009, **58**, 103–109.
- D. Zhang, C. Zhou, Z. Sun, L. Z. Wu, C. H. Tung and T. Zhang, *Nanoscale*, 2012, **4**, 6244–6255.

- 22 F. Zamani and S. M. Hosseini, *Catal. Commun.*, 2014, **43**, 164–168.
- 23 B. Deshmukh and M. V. Shelke, *RSC Adv.*, 2013, **3**, 21390–21393.
- 24 M. Beygzadeh, A. Alizadeh, M. M. Khodaei and D. Kordestani, *Catal. Commun.*, 2013, **32**, 86–91.
- 25 R. Rahimi, A. Maleki, S. Maleki, A. Morsali and M. J. Rahimi, *Solid State Sci.*, 2014, **28**, 9–13.
- 26 F. Zamani and E. Izadi, *Catal. Commun.*, 2013, **42**, 104–108.
- 27 A. F. Shojaei, K. Tabatabaeian, F. Shirini and S. Z. Hejazi, *RSC Adv.*, 2014, **4**, 9509–9516.
- 28 H. Woo and K. H. Park, *Catal. Commun.*, 2014, **46**, 133–137.
- 29 A. Maleki, N. Ghamari and M. Kamalzare, *RSC Adv.*, 2014, **4**, 9416–9423.
- 30 H. Yang, S. Li, X. Wang, F. Zhang, X. Zhong, Z. Dong and J. Ma, *J. Mol. Catal. A: Chem.*, 2012, **363–364**, 404–410.
- 31 S. R. Cherkupally and R. Mekala, *Chem. Pharm. Bull.*, 2008, **56**, 1002–1004.
- 32 R. Surasani, D. Kalita, A. V. D. Rao, K. Yarbaki and K. B. Chandrasekhar, *J. Fluorine Chem.*, 2012, **135**, 91–96.
- 33 J. Safari, S. Banitaba and S. D. Khalili, *Chin. J. Catal.*, 2011, **32**, 1850–1855.
- 34 R. Tafer, R. Boulcina, B. Carboni and A. Debache, *J. Chin. Chem. Soc.*, 2012, **59**, 1555–1560.
- 35 A. Heydari, S. Khaksar, M. Tajbakhsh and H. R. Bijanzadeh, *J. Fluorine Chem.*, 2009, **130**, 609–614.
- 36 B. Maleki, R. Tayebbe, Z. Sepehr and M. Kermanian, *Acta Chim. Slov.*, 2012, **59**, 814–823.
- 37 A. Mobinikhaledi, N. Foroughifar, M. A. B. Fard, H. Moghanian, S. Ebrahimi and M. Kalhor, *Synth. Commun.*, 2009, **39**, 1166–1174.
- 38 A. Debache, W. Ghalem, R. Boulcina, A. Belfaitah, S. Rhouati and B. Carboni, *Tetrahedron Lett.*, 2009, **50**, 5248–5250.
- 39 C. A. Antonyraj and S. Kannan, *Appl. Catal., A*, 2008, **338**, 121–129.
- 40 M. Adharvana Chari and K. Syamasundar, *Catal. Commun.*, 2005, **6**, 624–626.